COMMUNICATIONS IN SCIENCE AND TECHNOLOGY
Homepage: cst.kipmi.or.id

Simultaneous photoelectrocatalytic hydrogen production and ammonia degradation using titania nanotube-based photoanodes

Tiur Elysabeth[a], Eniya Listiani Dewi[b], Ratnawati[c], Kamarza Mulia[d], Slamet[d,*]

[a]*Department of Chemical Engineering, Faculty of Engineering, Universitas Serang Raya, Serang 42162, Indonesia*
[b]*Directorate General of New, Renewable Energy, and Energy Conservation, Ministry of Energy and Mineral Resources (KESDM), Jakarta Pusat, 10110, Indonesia*
[c]*Department of Chemical Engineering, Institut Teknologi Indonesia, Tangerang Selatan 15320, Indonesia*
[d]*Department of Chemical Engineering, Faculty of Engineering, Universitas Indonesia, Depok 16424, Indonesia*

Article history:
Received: 25 June 2024 / Received in revised form: 7 August 2024 / Accepted: 18 August 2024

Abstract

The primary focus of this research is to enhance the efficiency and effectiveness of the photoanode based of titania nanotubes in the photoelectrocatalytic process, which enables the simultaneous generation of hydrogen and degradation of ammonia. The modification process involved the incorporation of nitrogen dopant during anodization and sensitization of CuO through Successive Ionic Layer Adsorption Reaction (SILAR). The results of this study showed that the introduction of N dopant led to a significant enhancement in both the ammonia elimination and the hydrogen production, as evidenced by 3N-TiNTAs achieving 74.4% and 561 mmol/m^2, respectively. Meanwhile, the highest hydrogen production was observed with 7CuO-TiNTAs at 910.14 mmol/m^2. The study revealed that N-TiNTAs exhibited superior performance in ammonia degradation; while CuO-TiNTAs showed higher hydrogen production rates. Furthermore, the mechanistic aspects of the study were also thoroughly examined.

Keywords: Nitrogen-doped, CuO sensitized, photoelectrocatalytic, hydrogen production, ammonia degradation

1. Introduction

Hydrogen is a highly promising environmentally friendly and clean alternative energy source. Its use as a fuel is particularly appealing considering that its combustion only produces water vapor, thereby reducing the number of pollutants released into the atmosphere. This then has made hydrogen an ideal choice for powering vehicles and fuel cells to generate electricity [1]. In addition, the energy output from the combustion of hydrogen surpasses that of other fuels such as methane, gasoline, and coal. Numerous countries, for this reason, have then witnessed a substantial surge in research endeavors focused on augmenting the hydrogen generation. However, to make hydrogen as a truly leading energy resource, it is deemed crucial to ascertain that it is generated efficiently and sustainably [2] There are a number of methods in hydrogen production, including fossil fuels reform [3], water electrolysis, biological processes, thermal decomposition, and biomass gasification. It is crucial to highlight that the hydrogen production through methods such as reform, thermal decomposition, and biological processes frequently produces carbon dioxide (CO_2) emission. Considering this, scientists worldwide have been actively working on advancing hydrogen production technology. Among the various methods, water splitting has emerged as the preferred technique for hydrogen production as it can produce no CO_2 emissions [1]. Numerous approaches to water splitting have then been developed with recent studies focused on the decomposition of ammonia as a means of producing hydrogen. The use of ammonia as a raw material for hydrogen production is particularly intriguing as it does not produce CO_2 and offers a solution for the waste problem[4]. Ammonia shows great potential as a viable source of hydrogen and may play a significant role in the future hydrogen economy. In comparison to methanol, ammonia in its liquid form contains a higher concentration of hydrogen with a weight percentage of 17.6% compared to 12.5% [5]. Additionally, the use of ammonia solution as an energy storage material for hydrogen production is highly attractive for its ability to be stored in smaller volumes and at lower pressures [6-8].

Various techniques have been employed to produce hydrogen from ammonia decomposition, such as electrolysis [9], catalyst utilization at elevated temperatures [10], and photocatalytic [6]. At this point, electrolysis requires a substantial amount of power to convert ammonia into hydrogen, highlighting a need to investigate more energy-efficient alternatives. Photocatalytic, on the other hand, offers a straightforward and environmentally friendly method that utilizes a simple reactor without producing any additional

* Corresponding author.
Email: slamet@che.ui.ac.id
https://doi.org/10.21924/cst.9.2.2024.1464

pollutants [11].

One limitation of this approach is the occurrence of recombination, which poses a challenge to its effectiveness. To address this issue, a potential solution involves the integration of photocatalytic and electrolysis, resulting in a hybrid process known as photoelectrocatalytic (PEC). A study conducted by Nemoto and colleagues in 2007 delved into the generation of hydrogen and nitrogen through the breakdown of an ammonia solution [6,12,13].

Titania nanotube arrays (TiNTAs) exhibit an excellent photocatalytic activity when utilized as a photoanode in the photoelectrocatalytic process. The efficient transportation of electrons to cathode is made possible by the substantial surface area and distinctive one-dimensional channel structure of the material. These characteristics contribute to its ability to effectively facilitate electron transport [14]. On the other hand, the titania nanotube exhibits a drawback in terms of a significant bandgap energy ranging from 3 to 3.2 eV, which limits its potential applications. It also suffers from a high rate of electron-hole recombination, later on hindering its efficiency in certain processes [15]. The photo response is restricted to the UV region, resulting in the diminished quantum efficiency of the photoelectrocatalytic reaction. This limitation hinders the overall effectiveness of the reaction process as the photons are utilized ineffectively beyond the UV range.

The alteration through the introduction of non-metal atoms refers to a technique used to adjust the absorbance of titania nanotubes towards a higher wavelength, thereby enhancing the photoelectrochemical capabilities. Among the various types of non-metallic elements investigated for this purpose, nitrogen stands out as the most effective option, primarily in view of its structural similarities to oxygen, including characteristics such as electronegativity, coordination number, and ionic radius [16]. The hybridization of the O 2p and N 2p orbitals leads to the creation of a novel energy level positioned higher than the valence band. This phenomenon then causes a decrease in bandgap energy and an increase in the reactivity of titania nanotubes under visible light irradiation [17].

The adsorption capacity of the photoanode is a crucial concern that requires attention. To ensure an efficient process of ammonia decomposition and hydrogen production, it is vital for the photoanode to possess an ability to effectively adsorb pollutants. Numerous research have focused on synthesizing metal oxides such as CuO, MgO, and ZnO as potential ammonia adsorbents [18]. Enhancing the adsorption capacity of the photoanode for ammonia and improving the performance of the photoelectrocatalytic can be achieved by incorporating CuO - a favorable option for doping TiO_2 owing to its abundant availability, eco-friendliness, cost-effectiveness, and remarkable electrical conductivity [19,20]. Furthermore, the limited bandgap exhibited by copper-based oxides with values around 2.0 eV for Cu_2O and 1.7 eV for CuO renders them valuable for their potential application as sensitizers under visible light irradiation [21]. The incorporation of CuO effectively enhances the photocatalyst's sensitivity to visible light exposure [22]. The exploration of efficient hydrogen production systems by means of the PEC method and organic waste treatment has garnered a significant attention from researchers [20,23-25]. The phenomenon of electron trapping is commonly witnessed upon the introduction of Cu-based oxides into TiO_2 substances, playing a vital role in preventing the recombination of electron-hole pairs [26-28].

The principal focus of this study is to compare the photoelectrocatalytic performance of nitrogen-doped and CuO-sensitized titania nanotube arrays. Both nitrogen doping and CuO sensitization have the potential to enhance photon absorption, thereby optimizing the electron excitation process and increasing the generation of OH radicals. For this, it is deemed necessary to compare the performance of these two modifications to determine the most effective titania nanotube modification. The comparative analysis will specifically focus on the hydrogen production through the ammonia degradation. The impact of loading urea as a nitrogen precursor and loading CuO as a sensitizer on photoelectrocatalytic hydrogen production will be thoroughly examined. Furthermore, this study provides evidence that nitrogen-doped titania exhibits a higher number of adsorbed water surfaces and hydroxyl groups, thereby enhancing its photocatalytic activity. It also demonstrates that the addition of CuO as a sensitizer can significantly increase the adsorption capacity of titania nanotubes for ammonia.

2. Materials and Methods

2.1. Nitrogen-doped titania nanotube (N-TiNTAs) synthesis

The titania nanotubes were synthesized and modified through the addition of N dopant in situ during the anodization of Ti plates obtained from Baoji Jinsheng Metal Material Co. Ltd. To obtain N-TiNTAs, titanium foil was subjected to anodization in a 60 ml electrolyte solution, consisting of glycerol, 0.5%wt ammonium fluoride, 25%wt aqueous, and varied concentrations of urea (0.1%wt, 0.2%wt, 0.3%wt, and 0.4%wt) [29-32]. The process was carried out for 120 minutes under a voltage of 50 V[33], utilizing a DC power source. The experimental setup included a two-electrode system using titanium foil as the anode and platinum foil as the cathode. Magnetic stirring was implemented to aid in the reaction progression. Following the anodization process, the sample underwent a 3-hour annealing process at 500°C to induce the crystalline stage. Before undergoing annealing, the specimen underwent a washing process using distilled water, followed by exposure to N_2 gas flowing at a rate of 60 mL/min. Subsequently, the temperature gradually decreased to room temperature. The method of synthesis and modification of titania nanotubes with N dopant can provide a controlled and systematic approach to enhance the properties of the nanotubes for various applications in nanotechnology and material science.

2.2. CuO depositing on titania nanotube (CuO-TiNTAs)

Copper (II) nitrate trihydrate served as the precursor for the synthesis of titanium dioxide nanotubes decorated with copper (CuO-TiNTAs). The introduction of copper into TiNTAs was achieved in situ using the Successive Ionic Layer Adsorption and Reaction (SILAR) technique. It began by

preparing a solution containing copper (II) nitrate at various concentrations (0.03 M, 0.04 M, 0.05 M, 0.07 M, and 0.10 M) in a 60 mL volume. The ultrasonic bath used for this purpose was the Telsonic TPC 015, operating at 200 W and 65 kHz. The amorphous TiNTAs were formed on both sides of the Ti foil by immersing it in the copper nitrate solution using the ultrasonic bath. Subsequently, the samples were rinsed for 10 seconds and allowed to dry at room temperature for 1 minute. To ensure a fixed deposition of copper, this process was repeated 20 times, constituting one SILAR period. Finally, the Cu-deposited titanium dioxide nanotubes were annealed at 500°C for three hours to enhance their structural and morphological properties.

2.3. Titania nanotube characterization

The morphological analysis of TiNTAs, N-TiNTAs, and CuO-TiNTAs was conducted using two different field emission scanning electron microscopes or FESEM (FEI Inspect F50 and JEOL JIB-4610F) as well as a transmission electron microscope (FEI Tecnai G2 20 S-Twin). To determine the composition of the samples, an energy-dispersive X-ray spectrometer (EDX) with Oxford's XMAX 50 detector was used. Additionally, the CuO content on the titania nanotubes was determined using X-ray fluorescence (XRF) with a Rigaku Supermini200 instrument and a scintillation counter (SC) for a wavelength range of 0.01 – 0.3 nm. For the measurement of the optical absorption spectra of the photoanodes in the 300–800 nm wavelength range, UV-DRS (Agilent Technologies Cary 40) was utilized. The estimation of the bandgap was achieved by calculating the Kubelka-Munk function to interpret the obtained spectra. To perform the crystallography analysis of the titanium dioxide nanotubes, X-ray diffraction (XRD) was carried out by means of a Shimadzu 7000 Maxima-X instrument operating at 40 kV and 30 mA with a scan rate of 2° min^{-1} over a scan range of 10–80°. The light source used for this analysis was Cu Kα (λ=0.15406 nm). Finally, the atomic sensitivity factors were used to estimate the O atom in a hydroxyl group through the elemental peak areas obtained from X-ray photoelectron spectroscopy (XPS) using the ULVAC-PHI Quantera II instrument.

2.4. Hydrogen productions and ammonia degradation

The process of hydrogen production via photoelectrocatalytic was carried out utilizing a PEC cell system, consisting of a number of essential components such as a thermocouple, a mercury lamp (Philips HPL-N 250 W/542 E40), and continuous stirring. To ensure optimal conditions for the reaction, the photoreactor was positioned within a box featuring reflective walls. The PEC system enabled the direct flow of argon gas (99.99%) to the Gas Chromatography (GC, Shimadzu GC 2014) column for analysis. The actual hydrogen production took place in a 225 ml solution of ammonia with a concentration of 500 mg/L with the photoanode being situated flat inside the photoreactor.

Throughout the experiment, the photoelectrocatalytic reaction was continuously conducted within 2 hours with samples being collected at 30-minute intervals to quantify the amount of H_2 generated. The UV-Vis Spectrophotometer was used to assess the remaining ammonia content in the system using the Nessler method. Furthermore, the levels of ammonia were periodically analyzed in batches to monitor any changes over time. During the experiment, to ensure the stability of the reaction environment, a pH meter (Horiba, PH110-KN) was utilized to measure both the pH level and oxidation-reduction potential (ORP) every half hour.

3. Results and Discussion

3.1. Analysis of titania nanotubes properties

The positioning of nanotubes on the surface of the titanium substrate is dependent upon the competitive reaction between the formation of an oxidation layer and chemical dissolution [34]. To verify that the structure of titania in the form of nanotubes remained unchanged with the introduction of urea as a nitrogen precursor, FESEM characterization was conducted. The morphology of nitrogen-doped TiNTAs was compared to that of undoped TiNTAs, as shown in Fig. 1, in which no alterations in morphology were observed. This indicates that the nanotubular structure can withstand the effects of doping and thermal treatment, even when a layer of nitrogen is present on the surface of the N-TiNTAs. The average inner diameter of TiNTAs was in the range of 96 to 160 nm, while that of N-TiNTAs was in the range of 72 to 153 nm. The inner diameter of N-TiNTAs was found to be smaller than that of TiNTAs, consistent with previous research [35]. The detection of the N signal occurred when N was introduced into the TiNTA matrix through anodization. The N element was derived from urea. Table 1 demonstrates an increase in the N content on the photoanode as the concentration of the N precursor, urea, increased. The higher the amount of urea added, the greater the amount of N deposited on the nanotube structure of titania.

Table 1. EDX N-TiNTAs results

	TiNTAs	1N-TiNTAs	2N-TiNTAs	3N-TiNTAs	4N-TiNTAs
Ti	67.78%	70.29%	70.17%	69.60%	66.58%
O	32.22%	26.27%	26.23%	26.66%	29.31%
N	0%	3.44%	3.60%	3.75%	4.11%

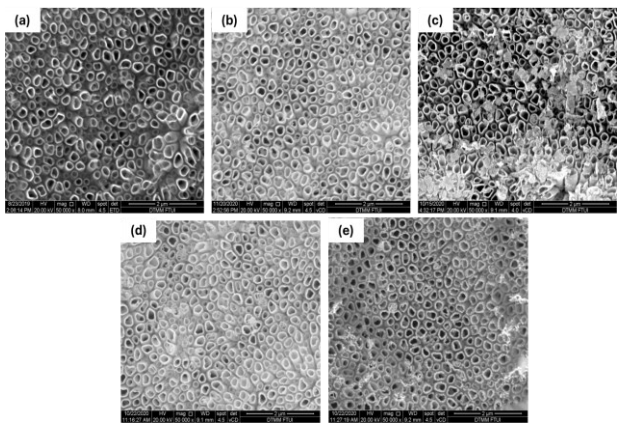

Fig. 1. FESEM images of (a) TiNTAs, (b) 1N-TiNTAs, (c) 2N-TiNTAs, (d) 3N-TiNTAs, and (e) 4N-TiNTAs

Fig. 2 shows the examination of the microstructures of CuO-TiNTAs, revealing that after the SILAR deposition process, CuO nanoparticles covered the surface of TiNTAs. The concentration of the precursor was found to have a significant impact on both the quantity and growth of the CuO deposited on the TiNTAs. This, as illustrated in Fig. 3, resulted in the sensitization of CuO on the TiNTAs surface where CuO nanoparticles were observed to be scattered across the surface. Moreover, an increase in precursor concentration led to a thickening of the tube wall, attributed to the higher amount of CuO attached on the TiNTAs surface, resulting in a uniform distribution of CuO nanoparticles on the nanotube surface. The SEM analysis further supported these findings by demonstrating that the tube wall thickness increased with the increasing concentration of the precursor. The EDX results also provided insights into the atomic concentration within the titania nanotubes at various concentrations of CuO precursors, as presented in Table 2. It was observed that a higher concentration of CuO precursor corresponded to a greater presence of Cu atoms in the titania nanotubes, reinforcing the relationship between the tube thickness and the increased amount of bound CuO. These results collectively underscore the influence of precursor concentration on the microstructure of CuO-TiNTAs, shedding light on the sensitization process and the distribution of CuO nanoparticles on the nanotube surface.

Furthermore, the correlation between the precursor concentration and the quantity of CuO bound was further confirmed through the XRF findings, in addition to the EDX outcomes. As presented in Table 3, an increase in the precursor concentration led to a corresponding rise in the weight percentage of CuO present within the titania nanotubes. Since Copper (II) nitrate trihydrate precursor was oxidized to CuO during the calcination process, the CuO content in TiNTAs was capable of representing the amount of Cu contained in TiNTAs.

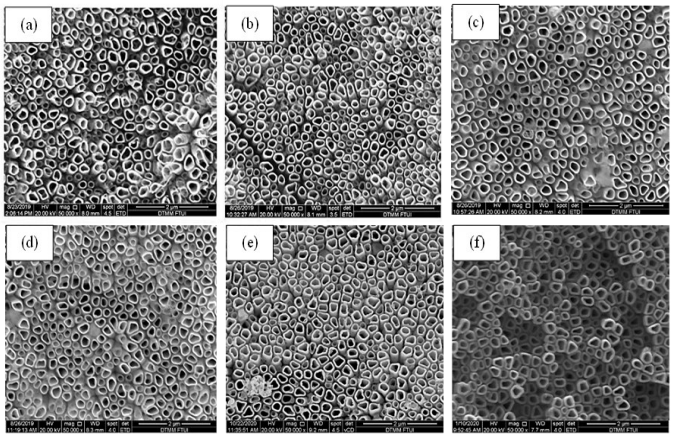

Fig. 2. Imaging of FESEM for (a) TiNTAs, (b) 3CuO-TiNTAs, (c) 4CuO-TiNTAs, (d) 5CuO-TiNTAs, (e) 7CuO-TiNTAs, and (f) 10CuO-TiNTAs

The uniformity of CuO particle distribution on the surface of the titania nanotubes was evident, as it extended consistently from the tube opening to the tube wall. This finding aligns with the findings from our previous research utilizing TEM analysis where a d-spacing value of 0.352 nm was linked to the d-spacing of TiO_2, specifically the crystal orientation of anatase (101) [36]. These results are consistent with the outcomes reported by Dandan et al [37]. Furthermore, the confirmation of CuO nanoparticles' presence is supported by a d-spacing value of 0.228 nm, particularly associated with the crystal orientation of CuO (002) nanoparticles. The crystal orientation (002) is characterized by a 2θ value of 35.63°, corresponding to the monoclinic CuO phase (JCPDS No. 02-1225) [38]. Fig. 3 presents the TEM images illustrating these findings, showcasing the distribution and crystal orientation of CuO particles on the titania nanotubes.

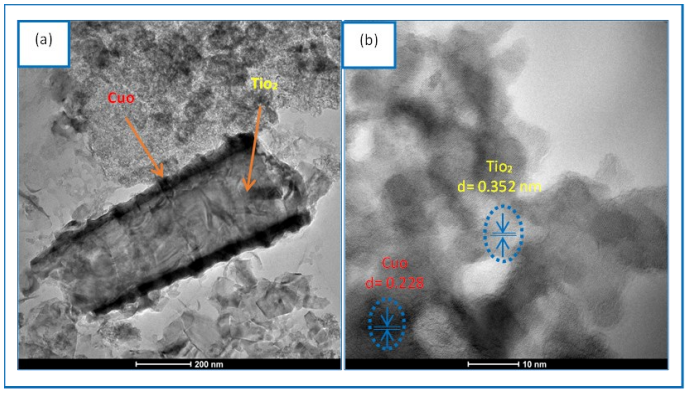

Fig. 3. (a) TEM and (b) HRTEM imaging for CuO-TiNTAs

Table 2. EDX results of CuO-TiNTAs

	TiNTAs	3CuO TiNTAs	4CuO TiNTAs	5CuO TiNTAs	7CuO TiNTAs	10CuO TiNTAs
Ti	67.78%	63.84%	74.12%	66.55%	68.32%	86.69%
O	32.22%	34.87%	24.47%	31.30%	29.45%	10.99%
Cu	0%	1.29%	1.41%	2.15%	2.22%	2.32%

Table 3. XRF results of CuO-TiNTAs

	TiNTAs	3CuO TiNTAs	4CuO TiNTAs	5CuO TiNTAs	7CuO TiNTAs	10CuO TiNTAs
TiO_2	100%	99.923%	99.921%	99.889%	99.864%	99.852%
CuO	0%	0.077%	0.079%	0.111%	0.136%	0.148%

The analysis of the crystal structure of titania nanotubes aimed to explore the impact of incorporating N and CuO on the inherent crystal properties of titania. It was executed using XRD (X-ray diffraction) technique. Fig. 4(a) presents the XRD pattern of N-TiNTAs and CuO-TiNTAs samples that underwent calcination at 500°C. The diffraction pattern revealed the presence of six signals at specific angles (2θ = 25.3°, 37.9°, 48.4°, 54.04°, 70.65°, and 76.20°), which corresponded to the crystal orientations of anatase phase, specifically (101), (004), (200), (105), (220), and (215) orientations, respectively. These orientations were identified based on the JCPDS No.21-1272 reference [39,40]. Interestingly, as shown in Fig. 2, the N atoms were uniformly distributed and only minimally dispersed within the TiNTAs matrix, resulting in the absence of a distinct diffraction peak for N [41]. The author can also do a deeper analysis based on the shifting of diffraction angle due to the effect of N doping. This analysis can provide more prove toward the successfully of N doping.

Fig. 4(b) demonstrates that the crystal structure of the titania nanotubes remained unchanged even after the

deposition of CuO. The XRD device was unable to detect the small quantity of CuO present on the surface of the titania nanotubes, resulting in the absence of a prominent signal from CuO crystals. This observation aligned with the results obtained from XRF and EDX analyses, confirming the minimal weight percentage of CuO and the highest concentration of elemental Cu. These findings collectively support the notion that the presence of CuO has no significant impact on the crystal structure of the titania nanotubes.

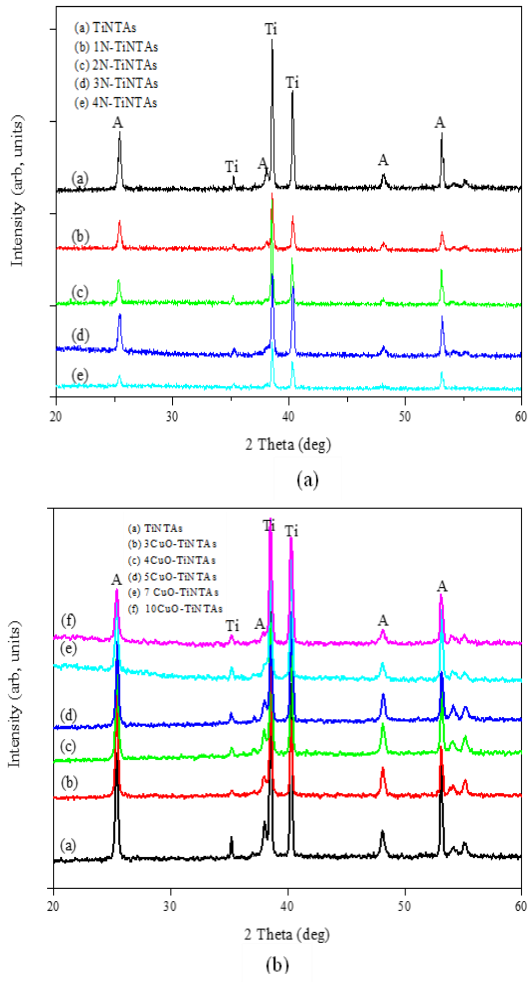

Fig. 4. XRD pattern for (a) N-TiNTAs and (b) CuO-TiNTAs

Fig. 5(a) informs the impact of nitrogen doped on the light absorption of TiNT. In the figure, the reflectance spectrum of N-TiNTAs displays a clear movement towards longer wavelengths. This suggests that nitrogen atoms can permeate the structure of TiNTAs and form N-Ti-O bonds. Previous studies have indicated that the choice of annealing gas has a significant impact on the formation of N-Ti-O bonds, leading to a reduction in the bandgap [42]. Annealing TiNTAs with N_2 gas resulted in a greater decrease in the energy of the band gap. Nitrogen gas can reduce the availability of oxygen in the calcination atmosphere, thereby reducing any unwanted oxidation reactions on the TiO_2 surface. This helps to keep the TiO_2 crystal structure stable and prevent unwanted phase changes. Nitrogen gas can help to remove any organic residues that may still exist on the TiO_2 surface after the calcination process. This is important to improve the quality and photocatalytic activity of TiO_2. As a result, the energy level in the valence band increases and the energy of the band gap decreases. The spectral range of 300 – 600 nm was investigated for optical absorption of the samples through the application of UV-Vis Diffuse Reflectance Spectroscopy (UV-Vis DRS). Fig. 5(a) and 5(b) illustrate the impact of N-doping on the optical absorption, revealing a shift in N-doping absorbance towards visible light. The band gap of the photoanode sample was determined using the Kubelka-Munk function and Tauc plot [43], and the results are presented in Table 4. The data indicated that 3N-TiNTAs exhibited the smallest bandgap energy, suggesting that 3N-TiNTAs require less energy to excite electrons from the valence band to the conduction band. Moreover, the low energy of the band gap enhances the efficiency of visible-light absorption. It is predicted that an increase in urea concentration correlates with an increase in molecular size, resulting in a reduced diffusion rate. This diminished diffusion rate subsequently led to a decrease in the quantity of nitrogen permeating the TiNTAs matrix, causing an accumulation of impurities on the surface, which in turn influenced the light irradiation process.

Table 4. N-TiNTAs bandgap energy calculation results

Photoanode	Bandgap energy (eV)
TiNTAs	3.17
1N- TiNTAs	3.07
2N- TiNTAs	2.99
3N- TiNTAs	2.95
4N- TiNTAs	3.02

The DRS UV-Vis characterization technique allowed for the measurement of the photon absorption spectra of TiNTAs and CuO-TiNTAs. Fig. 5(c) reveals that TiNTAs had an ability to absorb light with a wavelength below 400 nm, which could be attributed to their wide band gap. Upon CuO sensitization, the range of visible light that could be absorbed by CuO-TiNTAs expanded, encompassing the entire visible spectrum. The absorption intensity was observed to increase as the concentration of CuO precursor increased. However, at a concentration of 0.10 M, the absorption intensity decreased that could be attributed to the shielding effect, wherein multiple CuO particles hindered the incoming photons from reaching the photo-active site of the photocatalyst [44].

Fig. 5(b) and 5(d) illustrate the calculation of the bandgap energy through the utilization of the Kubelka-Munk plot [45,46]. The bandgap energy of TiNTAs was estimated to be around 3.17 eV, which aligned closely with the reference value of 3.20 eV for anatase. Table 5 presents the complete value for the bandgap energy. An essential characteristic of the CuO-TiNTAs bandgap is its capability to absorb photons with low energy and facilitate electron excitation at smaller energies. This property contributes to the advantageous thermodynamic properties required for efficient photoelectrocatalytic hydrogen production [24].

Table 5. CuO-TiNTAs bandgap energy calculation results

Photoanode	Bandgap energy (eV)
3CuO-TiNTAs	2.44
4CuO-TiNTAs	2.19
5CuO-TiNTAs	2.13
7CuO-TiNTAs	2.11
10CuO-TiNTAs	2.78

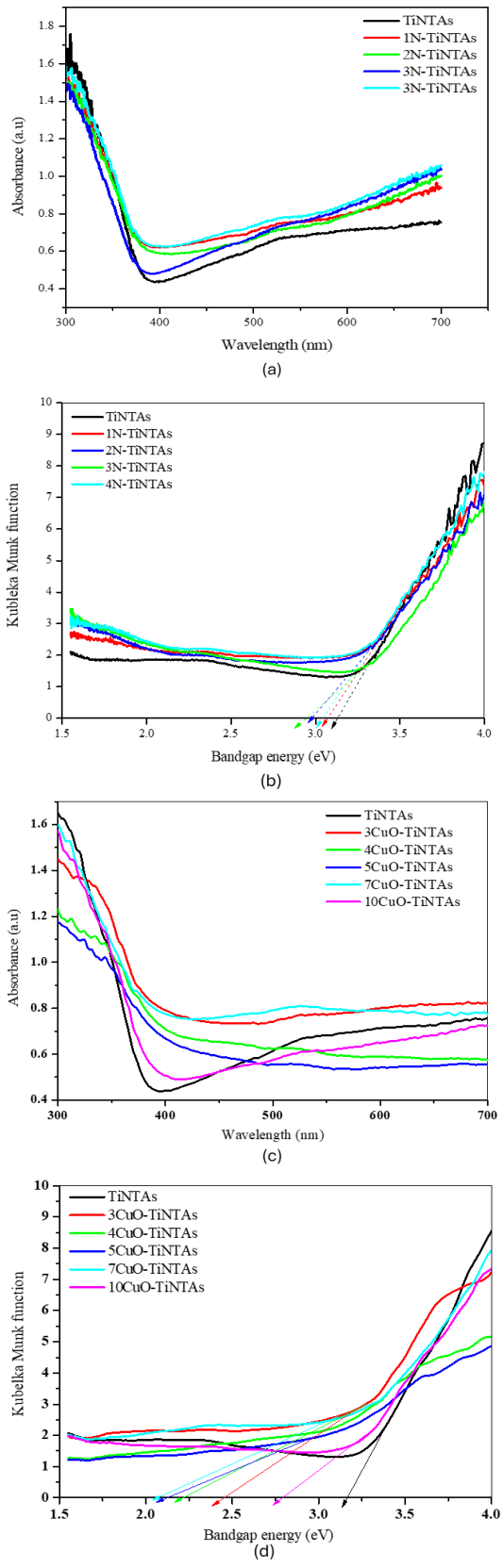

Fig. 5. (a, c) UV-Vis DRS spectrum reflectance and (b, d) Kubelka Munk plot

Based on the XPS characterization results as depicted in Fig. 6, it was possible to discern a rise in the quantity of hydroxyl groups. The characterization revealed the presence of surface hydroxyl groups and adsorbed oxygen from water molecules at 531 and 532 eV [45]. The comparison between the N-TiNTAs and CuO-TiNTAs demonstrated a disparity in the intensities of the hydroxyl groups formed. Notably, the intensity of the O atoms within the hydroxyl group of the N-TiNTAs surpassed that of the CuO-TiNTAs. This finding provides evidence that the incorporation of a nitrogen dopant can lead to an augmentation in the number of hydroxyl groups. The XPS measurements further indicated that the concentrations of O atoms within the hydroxyl groups of CuO-TiNTAs and N-TiNTAs were 20.47% and 60.60%, respectively.

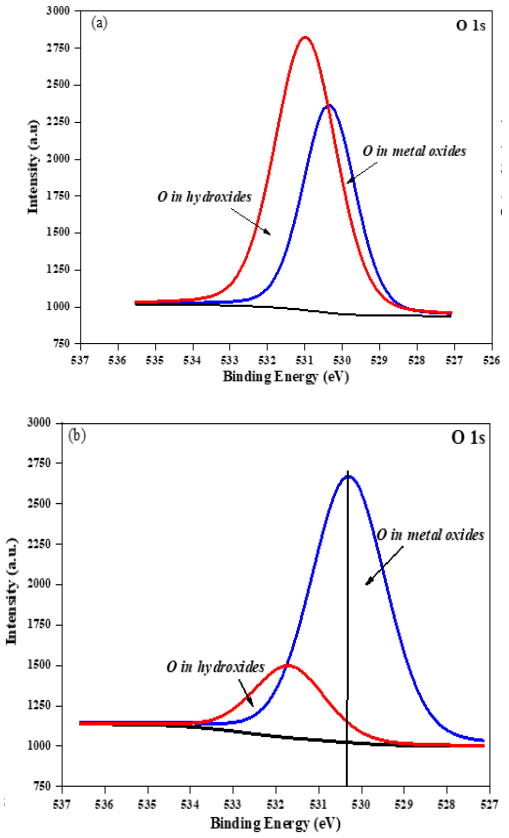

Fig. 6. Peak areas of XPS O 1s for (a) N-TiNTAs and (b) CuO-TiNTAs

3.2. Performance of photoanode to ammonia degradation by photoelectrocatalytic

Fig. 7(a) illustrates the degradation of ammonia over time and presents an analysis of the efficiency of different photoanode samples, such as TiNTAs and N-TiNTAs with varying levels of urea loading. Within a 120-minute timeframe, it was observed that 3N-TiNTAs exhibited the highest removal rate for ammonia at 74.4%, surpassing the removal rates of 31.1%, 35.1%, 55.8%, and 40.7% achieved by TiNTAs, 1N-TiNTAs, 2N-TiNTAs, and 4N-TiNTAs, respectively. The experimental results indicated that the performance of the photoanode specimens, particularly in terms of ammonia removal, was determined by the urea loading levels. The findings suggested that 3N-TiNTAs exhibited superior efficiency in removing ammonia compared to other specimens with different urea loadings. Moreover, the data revealed that, while higher urea loading generally led to increased ammonia removal rates, there were instances, such as in the case of 4N-TiNTAs where this trend was inconsistent. The findings highlighted the significance of considering the influence of urea loading on the efficiency of

photoanode materials in applications related to ammonia degradation.

The results obtained in this study align with the characterization of the samples in terms of their physical structure, crystal structure, and optical properties, which were previously discussed in the subsection. The findings in the analysis of the Energy Dispersive X-ray Spectroscopy (EDX) revealed that the samples of 3N-TiNTAs exhibited a higher nitrogen (N) content in contrast to the remaining samples. Furthermore, the determination of the bandgap energy using the Kubelka-Munk function equation demonstrated that the 3N-TiNTAs sample possessed the lowest bandgap energy among all the samples. Consequently, this sample exhibited a greater ability to absorb photon energy and generated a more efficient electron excitation. Moreover, the presence of hydroxyl groups in the N-TiNTAs material facilitated the capture of electron vacancies, resulting in the formation of hydroxyl radicals [47]. The accumulation of hydroxyl radicals was particularly advantageous in the process of ammonia degradation since hydroxyl radicals (•OH) served as the primary oxidizing agents during this degradation process. The reported reaction rate constant for the degradation of ammonia by hydroxyl radicals (•OH) is 1 x 10^8 M^{-1} sec^{-1} [48]. Therefore, the increased formation of hydroxyl radicals in the N-TiNTAs material enhances its potential for efficient ammonia degradation.

Fig. 7(b) depicts the degradation of ammonia through photoelectrocatalytic means over a specific timeframe, showing the performance of various photoanode samples such as TiNTAs, 3CuO-TiNTAs, 4CuO-TiNTAs, 5CuO-TiNTAs, 7CuO-TiNTAs, and 10CuO-TiNTAs. Of these samples, 3CuO-TiNTAs was observed to have the highest degradation of ammonia with at 50.1% within 120 minutes, exceeding the results obtained with TiNTAs, 4CuO-TiNTAs, 5CuO-TiNTAs, 7CuO-TiNTAs, and 10CuO-TiNTAs, which yielded the degradation percentages of 31.1%, 45.29%, 43.51%, 41.33%, and 30.11% respectively. The presence of CuO nanoparticles on the surface of titania nanotubes could enhance the absorption of visible light due to the fact that the conduction band (CB) of CuO with a value of -0.8 eV is more negative compared to the CB of TiO_2, which stands at -0.4 eV. When exposed to light, electrons are generated in the CB of CuO and then transferred to the CB of TiO_2. Conversely, the energy level of the valence band (VB) of CuO, which is +0.9 eV, is higher than that of TiO_2, which is +2.8 eV, allowing the holes produced in TiO_2 to accumulate in the VB of CuO. This accumulation of holes in the VB of CuO facilitates the oxidation process, as indicated by previous studies [24]. It is apparent that incorporating copper (Cu) into the titania nanotubes (TiNTAs) surfaces results in the increased adsorption of ammonia, thus improving the efficiency of ammonia photodegradation [49]. The presence of 3CuO-TiNTAs, 4CuO-TiNTAs, 5CuO-TiNTAs, and 7CuO-TiNTAs results in a higher percentage of ammonia removal compared to TiNTAs, confirming this observation. However, the percentage of ammonia removal is lower in 10CuO-TiNTAs when compared to TiNTAs. This can be attributed to the photoanode of 10CuO-TiNTAs, which exhibits a shielding effect and hampers the absorption of visible light, thereby reducing its effectiveness.

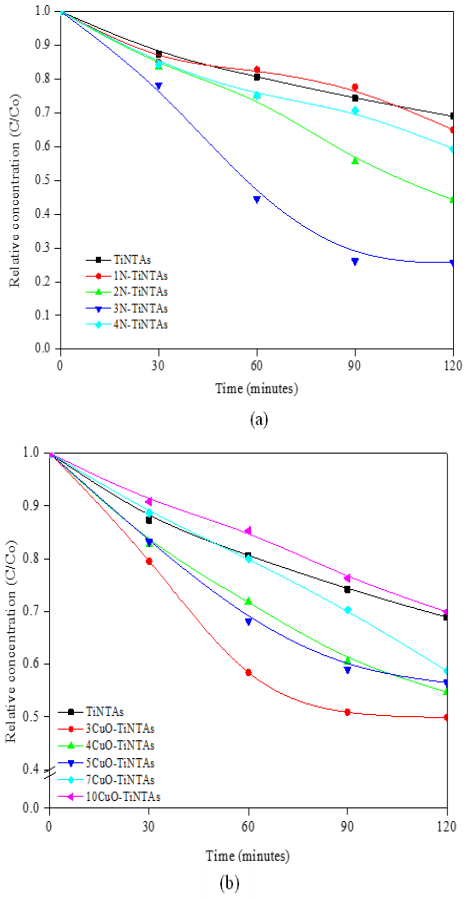

Fig. 7. NH_3 photoelectrocatalytic degradation using various photoanodes (a) N-TiNTAs and (b) CuO-TiNTAs

The degradation of ammonia in all CuO-TiNTAs photoanodes exhibited a decrease in yield, which was found to be inversely proportional to the loading of CuO. The presence of a higher amount of CuO on the surface of the titania nanotube hindered the entry of ammonia onto the surface, thus resulting in a reduced degradation efficiency. The loss of ammonia can be attributed to a combined effect of adsorption and degradation processes, working synergistically to remove the ammonia from the system [50].

3.3. Effect of loading urea and CuO on hydrogen production by photoelectrocatalytic

The experiment aimed to determine the photoelectrocatalytic performance of ammonia degradation to H_2. This evaluation was conducted by utilizing an ammonia solution and subjecting it to the illumination of a 250W Mercury Lamp (320 – 700 nm). As a benchmark, the performance of TiNTAs was also evaluated in which its outcomes are presented in Fig. 8, depicting the impact of illumination time on the quantity of H_2 generated. Additionally, Fig. 8(a) showcases a comparison between the H_2 production results of N-TiNTAs and TiNTAs. Notably, the maximum H_2 production yield of 561 mmol/m^2 was achieved by 3N-TiNTAs, exhibiting a four-fold increase in activity compared to TiNTAs (127 mmol/m^2). Conversely, the activity of 4N-TiNTAs decreased to 240 mmol/m^2. The significant enhancement in the activity of nitrogen-doped titania nanotubes (N-TiNTAs) can be attributed to the augmented

absorption resulting from nitrogen doping and the heightened charge transfer within the N-TiNTAs.

The enhanced photocatalytic performance of the titania synthesized using this method can be attributed to its increasing sensitivity to visible light. The UV-DRS spectra analysis revealed that the N-TiNTA photoanodes displayed enhanced absorption within the visible light spectrum when compared to the undoped titania nanotubes. This indicates that the introduction of nitrogen doping leads to a reduction in the band gap of the titania nanotubes, resulting in the formation of impurity levels. Consequently, the photoanode is capable of efficiently absorbing a significant portion of the solar spectrum, enabling excitation by low-energy photons for ammonia degradation. In addition to the improved absorption, the enhanced activity of the N-TiNTAs sample can be attributed to the formation of multiple phases, which significantly reduces the recombination of hole-electron pairs. In the photoelectrochemical response test, Reddy et al. (2017) conducted a study on N-doped TiO_2 photocatalysis and observed a comparable phenomenon [51]. The findings revealed that the presence of an optimal quantity of nitrogen facilitates charge transfer. However, an excessive amount of nitrogen leads to a shielding effect, wherein numerous nitrogen particles hinder the photon from reaching the photo-active site of the photocatalyst. Furthermore, an excessive concentration of nitrogen precursors results in the coverage of the tube surface, thereby obstructing the incoming light.

Fig. 8(b) depicts the utilization of TiNTAs as control samples and CuO-TiNTAs photoanodes illustrating the process of hydrogen production. The results indicated that the presence of CuO on the titania nanotubes enhanced the activity of hydrogen production. This enhancement was attributed to the improved charge transfer and separation efficiency facilitated by the deposition of CuO, leading to an increase in the amount of hydrogen generated at the cathode.

Also, as depicted in Fig. 8(b), the 7CuO-TiNTAs samples exhibited a greater hydrogen production in comparison to the remaining samples. The hydrogen production reached a maximum value of 910.14 mmol/m2 within 120 minutes. This finding highlights the significant influence of the photoanodic characteristics of CuO loading on titania nanotubes in the hydrogen production. As the CuO loading increases, the number of electrons donated to the conduction band of the titania nanotubes increases as well. This is crucial for the cathode to receive adequate electrons to effectively reduce all the H^+ ions produced through either water hydrolysis or ammonia breakdown. Additionally, the 7CuO-TiNTAs samples exhibited a lower bandgap energy, resulting in an excellent response to photons. This then led to the excitation of a greater number of electrons from the valence band. On the other hand, the 10CuO-TiNTAs photoanodes demonstrated a distinct trend. The excessive loading of 0.10 M CuO precursor led to a wall thickness exceeding the maximum limit. Consequently, the accumulation of CuO particles then created a shielding effect, where the particles essentially covered one another, resulting in suboptimal light absorption.

The photocatalytic process is hindered by a significant chance of hole-electron recombination, resulting in reduced efficiency. However, this drawback can be addressed by employing a photoelectrocatalytic process, enabling more efficient charge transfer. As a result, the degradation process and hydrogen production can be enhanced, as supported by references [48,52,53].

Another aim of this study is to demonstrate that the inclusion of CuO as a sensitizer has a significant impact on enhancing the adsorption capability of titania nanotubes towards ammonia. This heightened adsorption capacity facilitates a more efficient degradation process of ammonia on the surface of the photocatalyst. As a result, an increased amount of ammonia is adsorbed onto the photocatalyst's surface, thereby providing a greater opportunity for it to react with OH• and undergo decomposition, ultimately releasing H^+.

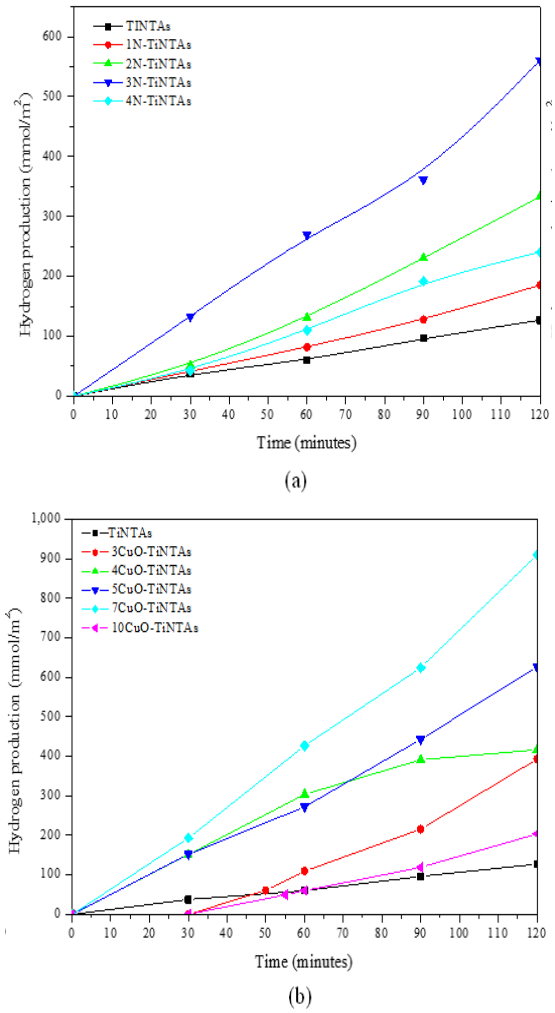

Fig. 8. Photoelectrocatalytic hydrogen production using various photoanodes (a) N-TiNTAs and (b) CuO-TiNTAs

The experiment involved conducting an ammonia adsorption test using CuO-TiNTAs in a PEC reactor, which was the similar reactor used for the ammonia degradation process. However, unlike the degradation process, no light was utilized in this stage. The initial concentration of ammonia used in the test was 500 mg/L. Fig. 9 illustrates that the addition of CuO sensitizer to titania nanotubes could enhance the adsorption capacity for ammonia. When compared to TiNTAs, the five samples of CuO-TiNTAs exhibited higher adsorption capacities. Notably, the 3CuO-TiNTAs photoanode demonstrated the highest maximum

adsorption capacity among the samples. This can be attributed to the fact that a higher concentration of CuO results in a thicker CuO layer on the surface of the titania nanotubes, which in turn covers the pores and hinders the entry of ammonia molecules onto the surface.

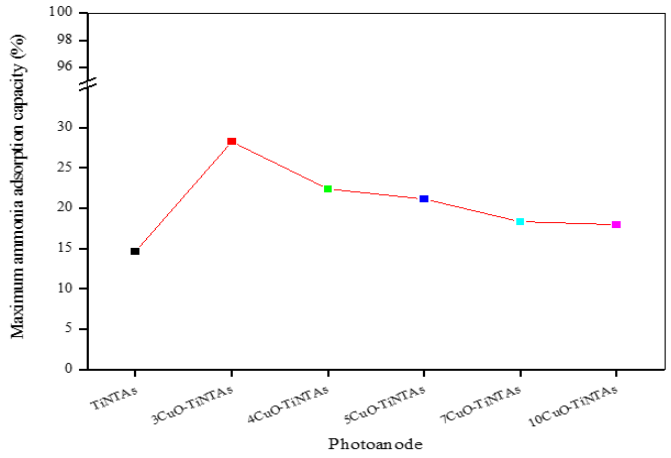

Fig. 9. Adsorption capacity of various photoanodes

3.4. Analysis of reaction mechanisms

Upon dissolution in water, the ammonium ions undergo a reaction pathway known as reaction path 1, which determines the balance. Under alkaline conditions, the equilibrium shifts towards the right, resulting in the formation of NH_3. Conversely, at low pH levels, the majority of ammonia exists in the form of ionized ammonium ions (NH_4^{+}) [54]. In the context of the degradation of ammonia through photoelectrocatalysis, the experiment was conducted at an alkaline pH of approximately 11. Over the course of the 2-hour reaction period, the pH of the solution decreased to around 10, leading to the dominance of the non-ionic form of ammonia. It is worth noting that NH_4^+ in its ionized form was considered inactive in compartment 1 of this study, as there were no available electrons to facilitate its reduction.

$$NH_4^+ + OH^- \rightleftarrows NH_3 + H_2O \quad (1)$$

The process of ammonia degradation results in the production of H^+ ions, which are formed by splitting of the ammonia structure. Numerous scientists have discovered that various active species, such as h^+ and OH•, act as the oxidizing agents during the photoelectrocatalytic ammonia degradation process [55,56].

The utilization of CuO as a sensitizer has been found to enhance the efficiency of the ammonia oxidation process by augmenting the adsorption capacity of ammonia. Consequently, this leads to an overall improvement in the efficiency of photodegradation, as highlighted in a previous study [49]. To provide a comprehensive overview, the subsequent discussion outlines the potential mechanisms involved in the photodegradation of ammonia [49]:

$$NH_{3(ad)} + h^+ \rightarrow \cdot NH_{2(ad)} + H^+ \quad (2)$$

$$NH_{3(ad)} + \cdot OH \rightarrow NH_2OH_{(ad)} + H^+ \quad (3)$$

$$NH_2OH_{(ad)} + h^+(or \cdot OH) \rightarrow \cdot NHOH_{(ad)} + H^+ (or\, H_2O) \quad (4)$$

$$\cdot NHOH_{(ad)} + \cdot NHOH_{(ad)} \rightarrow N_{2\,(ad)} + 2H_2O \quad (5)$$

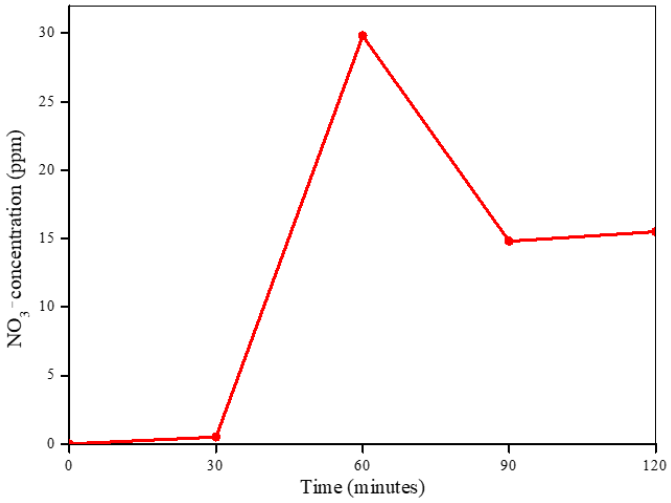

Fig. 10. NO_3^- concentration along the reaction

The identification of intermediate compounds occurred during the ammonia degradation revealed the presence of NO_3^- ions. The analysis of these intermediate compounds was conducted at 30 minutes intervals during the degradation process, resulting in the observation of a decreasing profile of NO_3^- ions in solution, as depicted in Fig. 10. The decrease in the concentration of NO_3^- ions after 60 minutes of reaction time indicates that NO_3^- serves as an intermediate compound that will undergo further degradation into other compounds.

During the degradation process of ammonia, if the presence of NO_2^- or NO_3^-ion species was detected, it was observed that NH_2OH could serve as an alternative intermediate. Furthermore, it is suggested that reactions 6 – 9 might be involved in certain reaction pathways.

$$\cdot NH_{2(ad)} + OH \cdot \rightarrow NH_2OH_{(ad)} \quad (6)$$

$$NH_2OH_{(ad)} + \cdot OH \rightarrow NO_2^- + H^+ \quad (7)$$

$$NO_2^- + \cdot OH \rightarrow HONO_2 \quad (8)$$

$$HONO_2 \rightarrow NO_3^- + H^+ \quad (9)$$

Yamazoe et al (2007) stated that the presence of NO_3^- species on the surface of TiO2 can undergo a reaction with NH_2 radicals, which are generated through the NH_3 degradation by OH radicals or h^+, resulting in the production of N_2. This phenomenon was observed through a spectrophotometric analysis where the concentration of NO_3^- was found to decrease over time until the reaction completed. The proposed mechanism by Yamazoe et al (2007) suggests that the formation of N_2 can continue through a series of steps [57].

$$\cdot NH_{2(ad)} + NO_{3\,(ad)} \rightarrow (NH_2NO_3) \rightarrow N_2 + H_2O + O_2 \quad (10)$$

Under the experimental conditions employed in this study, it is possible to propose a mechanism for the ammonia degradation through photoelectrocatalysis, as depicted in reactions 2 – 10.

The introduction of dopant N has a capability to enhance the concentration of OH^- ions, thereby leading to a greater likelihood of ammonia structure breakdown, primarily driven by the oxidizing agent OH^-. It is worth noting that the rate constant for the degradation of NH_3 by OH^- is higher compared to that of h^+ with a value of approximately 1 x 10^8 M^{-1} sec^{-1} [48].

4. Conclusion

The synthesis of N-TiNTAs photoanodes was successfully achieved through an in-situ method during the anodization process. The characterization results indicated that the resulting N-TiNTAs displayed superior photoelectrochemical properties and responses. Meanwhile, the photoelectrocatalysis tests for ammonia degradation and hydrogen production demonstrated that 3N-TiNTAs had the highest percentage of ammonia removal at 74.4% and hydrogen production at 561.12 mmol/m^2. This highlighted the efficiency of 3N-TiNTAs in these processes. By varying the CuO precursor loading using the SILAR method, CuO-TiNTAs were tailored to achieve optimal CuO loading with enhanced characteristics and performance. The characterization of the photoanodes revealed that 7CuO-TiNTAs exhibited superior characteristics compared to other variations. Performance tests further confirmed the unique properties of CuO-TiNTAs with 3CuO-TiNTAs showing the highest adsorption capacity at 28.25% and 50.1% ammonia removal. Notably, 7CuO-TiNTAs demonstrated the highest hydrogen production at 910.14 mmol/m^2, underscoring their efficiency in this aspect. The findings of this investigation revealed that titania nanotubes doped with nitrogen and sensitized with CuO exhibited superior performance compared to unaltered titania nanotubes.

Acknowledgements

The financial backing for this project is provided through the PDUPT Grant, which is administered by the Directorate of Research, Technology, and Community Service under the Directorate General of Higher Education, Research, and Technology. This grant is awarded by the Ministries of Education, Culture, Research, and Technology, and the contract number for this project is NKB-914/UN2.RST/HKP.05.00/2023.

References

1. Huang D-C, Jiang C-H, Liu F-J, Cheng Y-C, Chen Y-C, Hsueh K-L. *Preparation of Ru–Cs catalyst and its application on hydrogen production by ammonia decomposition*. Int J Hydrogen Energy.38(8) (2013) 3233-40.
2. Luo M, Yi Y, Wang S, Wang Z, Du M, Pan J, et al. *Review of hydrogen production using chemical-looping technology*. Renew Sustainable Energy Rev.81 (2018) 3186-214.
3. Yin S-F, Zhang Q-H, Xu B-Q, Zhu W-X, Ng C-F, Au C-T. *Investigation on the catalysis of COx-free hydrogen generation from ammonia*. J Catal.224(2) (2004) 384-96.
4. Yin SF, Xu BQ, Zhu WX, Ng CF, Zhou XP, Au CT. *Carbon nanotubes-supported Ru catalyst for the generation of COx-free hydrogen from ammonia*. Catal Today.93-95 (2004) 27-38.
5. Giddey S, Badwal SPS, Kulkarni A. *Review of electrochemical ammonia production technologies and materials*. Int J Hydrogen Energy.38(34) (2013) 14576-94.
6. Nemoto J, Gokan N, Ueno H, Kaneko M. *Photodecomposition of ammonia to dinitrogen and dihydrogen on platinized TiO2 nanoparticules in an aqueous solution*. Photochem Photobiol A: Chem.185(2) (2007) 295-300.
7. Maffei N, Pelletier L, Charland JP, McFarlan A. *An intermediate temperature direct ammonia fuel cell using a proton conducting electrolyte*. J Power Sources.140(2) (2005) 264-7.
8. Pelletier L, McFarlan A, Maffei N. *Ammonia fuel cell using doped barium cerate proton conducting solid electrolytes*. J Power Sources.145(2) (2005) 262-5.
9. Vitse F, Cooper M, Botte GG. *On the use of ammonia electrolysis for hydrogen production*. J Power Sources.142(1-2) (2005) 18-26.
10. Podila S, Driss H, Zaman SF, Ali AM, Al-Zahrani AA, Daous MA, et al. *Effect of preparation methods on the catalyst performance of Co/MgLa mixed oxide catalyst for COx-free hydrogen production by ammonia decomposition*. Int J Hydrogen Energy.42(38) (2017) 24213-21.
11. Rini AS, Nabilla A, Rati Y. *Microwave-assisted biosynthesis and characterization of ZnO film for photocatalytic application in methylene blue degradation*. Communications in Science and Technology.6(2) (2021) 69-73.
12. Talat-Mehrabad J, Khosravi M, Modirshahla N, Behnajady MA. *Sol–gel preparation and characterization of Ag and Mg co-doped nano TiO2: efficient photocatalytic degradation of C.I. Acid Red 27*. Res Chem Intermed.42(2) (2016) 595-609.
13. Pan X, Xie Q, Chen W-l, Zhuang G-l, Zhong X, Wang J-g. *Tuning the catalytic property of TiO2 nanotube arrays for water splitting*. Int J Hydrogen Energy.38(5) (2013) 2095-105.
14. Lee K, Mazare A, Schmuki P. *One-Dimensional Titanium Dioxide Nanomaterials: Nanotubes*. Chem Rev.114(19) (2014) 9385-454.
15. Slamet S, Pelawi LF, Ibadurrohman M, Yudianti R, Ratnawati R. *Simultaneous Decolorization of Tartrazine and Production of H2 in a Combined Electrocoagulation and Photocatalytic Processes using CuO-TiO2 Nanotube Arrays: Literature Review and Experiment*. Indones J Sci Technol.7(3) 385-404.
16. Chen X, Burda C. *The electronic origin of the visible-light absorption properties of C-, N-and S-doped TiO2 nanomaterials*. J Am Chem Soc.130(15) (2008) 5018-9.
17. Asahi R, Morikawa T, Ohwaki T, Aoki K, Taga Y. *Visible-light photocatalysis in nitrogen-doped titanium oxides*. Science.293(5528) (2001) 269-71.
18. Rezaei E, Schlageter B, Nemati M, Predicala B. *Evaluation of metal oxide nanoparticles for adsorption of gas phase ammonia*. J Environ Chem Eng.5(1) (2017) 422-31.
19. Momeni MM. *Fabrication of copper decorated tungsten oxide–titanium oxide nanotubes by photochemical deposition technique and their photocatalytic application under visible light*. Appl Surf Sci.357 (2015) 160-6.
20. Momeni MM, Ghayeb Y, Ezati F. *Fabrication, characterization and photoelectrochemical activity of tungsten-copper co-sensitized TiO2 nanotube composite photoanodes*. J Colloid Interface Sci.514 (2018) 70-82.
21. Sun Q, Li Y, Sun X, Dong L. *Improved Photoelectrical Performance of Single-Crystal TiO2 Nanorod Arrays by Surface Sensitization with*

Copper Quantum Dots. ACS Sustainable Chem Eng.1(7) (2013) 798-804.

22. Husein S, Rustamadji RR, Pratiwi R, Dewi EL. *Simultaneous tartrazine-tetracycline removal and hydrogen production in the hybrid electrocoagulation-photocatalytic process using g-C3N4/TiNTAs*. Communications in Science and Technology.9(1) (2024) 46-56.
23. Zhong JS, Wang QY, Zhou J, Chen DQ, Ji ZG. *Highly efficient photoelectrocatalytic removal of RhB and Cr(VI) by Cu nanoparticles sensitized TiO2 nanotube arrays*. Appl Surf Sci.367 (2016) 342-6.
24. Hua Z, Dai Z, Bai X, Ye Z, Wang P, Gu H, et al. *Copper nanoparticles sensitized TiO2 nanotube arrays electrode with enhanced photoelectrocatalytic activity for diclofenac degradation*. Chem Eng J.283 (2016) 514-23.
25. Zhang L, Cao H, Pen Q, Wu L, Hou G, Tang Y, et al. *Embedded CuO nanoparticles@TiO2-nanotube arrays for photoelectrocatalytic reduction of CO2 to methanol*. Electrochim Acta.283 (2018) 1507-13.
26. Lei M, Wang N, Zhu L, Zhou Q, Nie G, Tang H. *Photocatalytic reductive degradation of polybrominated diphenyl ethers on CuO/TiO2 nanocomposites: A mechanism based on the switching of photocatalytic reduction potential being controlled by the valence state of copper*. Appl Catal B: Environ.182 (2016) 414-23.
27. Hassan NS, Jalil AA, Triwahyono S, Hitam CNC, Rahman AFA, Khusnun NF, et al. *Exploiting copper–silica–zirconia cooperative interactions for the stabilization of tetragonal zirconia catalysts and enhancement of the visible-light photodegradation of bisphenol A*. J Taiwan Inst Chem Eng.82 (2018) 322-30.
28. Zangeneh H, Farhadian M, Zinatizadeh AA. *N (Urea) and CN (L-Asparagine) doped TiO2-CuO nanocomposites: Fabrication, characterization and photodegradation of direct red 16*. J Environ Chem Eng.8(1) (2020) 103639.
29. Roy P, Berger S, Schmuki P. *TiO2 nanotubes: synthesis and applications*. Angew Chem Int Ed.50(13) (2011) 2904-39.
30. Ratnawati, Gunlazuardi J, Slamet. *Synthesis of TiO2 Nanotube Arrays by Sonication Aided Anodization and Its Application for Hydrogen Generation from Aqueous Glycerol Solution*. MATEC Web Conf.28 (2015) 01001.
31. Ratnawati, Gunlazuardi J, Dewi EL, Slamet. Int J Hydrogen Energy.39 (2014) 16927-35.
32. Gunlazuardi J. *Development of titania nanotube arrays: The roles of water content and annealing atmosphere*. Mater Chem Phys.160 (2015) 111-8.
33. Ratnawati R, Gunlazuardi J, Slamet S. Effect of Anodization Time and Temperature on the Morphology of TiO2 Nanotube Arrays for Photocatalytic Hydrogen Production from Glycerol Solution2014: Proceeding the Regional Conference on Chemical Engineering.
34. Liang H-c, Li X-z. *Effects of structure of anodic TiO2 nanotube arrays on photocatalytic activity for the degradation of 2, 3-dichlorophenol in aqueous solution*. J Hazard Mater.162(2-3) (2009) 1415-22.
35. Elysabeth T, Slamet, Sri Redjeki A. *Effect of urea loading on the anodic synthesis of titania nanotube arrays photoanode to enhance photoelectrochemical performance*. IOP Conf Ser: Mater Sci Eng.509 (2019).
36. Elysabeth T, Mulia K, Ibadurrohman M, Dewi EL, Slamet. *A comparative study of CuO deposition methods on titania nanotube arrays for photoelectrocatalytic ammonia degradation and hydrogen production*. Int J Hydrogen Energy.46(53) (2021) 26873-85.
37. Cao D, Wang Q, Zhu S, Zhang X, Li Y, Cui Y, et al. *Hydrothermal construction of flower-like MoS2 on TiO2 NTs for highly efficient environmental remediation and photocatalytic hydrogen evolution*. Sep Purif Technol.265 (2021) 118463.
38. Bouazizi N, Bargougui R, Oueslati A, Benslama R. *Effect of synthesis time on structural, optical and electrical properties of CuO nanoparticles synthesized by reflux condensation method*. Adv Mater Lett.6(2) (2015) 158-64.
39. Meng A, Zhang J, Xu D, Cheng B, Yu J. *Enhanced photocatalytic H2-production activity of anatase TiO2 nanosheet by selectively depositing dual-cocatalysts on {101} and {001} facets*. Appl Catal B: Environ.198 (2016) 286-94.
40. Deng F, Luo X, Shu H, Tu X, Luo S. *Synthesis of anatase TiO2 in a vinyl-containing ionic liquid and its enhanced photocatalytic activity*. Res Chem Intermed.39(6) (2013) 2857-65.
41. Luo N, Jiang Z, Shi H, Cao F, Xiao T, Edwards PP. *Photo-catalytic conversion of oxygenated hydrocarbons to hydrogen over heteroatom-doped TiO2 catalysts*. Int J Hydrogen Energy.34(1) (2009) 125-9.
42. Elysabeth T, Slamet, Sri Redjeki A. *Synthesis of N doped titania nanotube arrays photoanode using urea as nitrogen precursor for photoelectrocatalytic application*. IOP Conf Ser: Mater Sci Eng; 2019: IOP Publishing.
43. Zhou L, Deng J, Zhao Y, Liu W, An L, Chen F. *Preparation and characterization of N–I co-doped nanocrystal anatase TiO2 with enhanced photocatalytic activity under visible-light irradiation*. Mater Chem Phys.117(2) (2009) 522-7.
44. Mukul M, Devi N, Sharma S, Tripathi SK, Rani M. *Synthesis and study of TiO2/CuO core shell nanoparticles for photovoltaic applications*. Mater Today Proc.28 (2020) 1382-5.
45. Liu Z, Song Y, Wang Q, Jia Y, Tan X, Du X, et al. *Solvothermal fabrication and construction of highly photoelectrocatalytic TiO2 NTs/Bi2MoO6 heterojunction based on titanium mesh*. J Colloid Interface Sci.556 (2019) 92-101.
46. Xing Y, Gao X, Ji G, Liu Z, Du C. *Synthesis of carbon doped Bi2MoO6 for enhanced photocatalytic performance and tumor photodynamic therapy efficiency*. Appl Surf Sci.465 (2019) 369-82.
47. Cheng X, Yu X, Xing Z. *Characterization and mechanism analysis of N doped TiO2 with visible light response and its enhanced visible activity*. Appl Surf Sci.258(7) (2012) 3244-8.
48. Xiao S, Wan D, Zhang K, Qu H, Peng J. *Enhanced photoelectrocatalytic degradation of ammonia by in situ photoelectrogenerated active chlorine on TiO2 nanotube electrodes*. J Environ Sci.50 (2016) 103-8.
49. Feng J, Zhang X, Zhang G, Li J, Song W, Xu Z. *Improved photocatalytic conversion of high−concentration ammonia in water by low−cost Cu/TiO2 and its mechanism study*. Chemosphere.274 (2021) 129689.
50. Liu W, Ni J, Yin X. *Synergy of photocatalysis and adsorption for simultaneous removal of Cr(VI) and Cr(III) with TiO_2 and titanate nanotubes*. Water Res.53 (2014) 12-25.
51. Reddy PAK, Reddy PVL, Kim K-H, Kumar MK, Manvitha C, Shim J-J. *Novel approach for the synthesis of nitrogen-doped titania with variable phase composition and enhanced production of hydrogen under solar irradiation*. Journal of Industrial and Engineering Chemistry.53 (2017) 253-60.
52. Zhai C, Zhu M, Bin D, Wang H, Du Y, Wang C, et al. *Visible-light-assisted electrocatalytic oxidation of methanol using reduced graphene oxide modified Pt nanoflowers-TiO2 nanotube arrays*. ACS applied materials & interfaces.6(20) (2014) 17753-61.
53. Zhai C, Zhu M, Lu Y, Ren F, Wang C, Du Y, et al. *Reduced graphene oxide modified highly ordered TiO 2 nanotube arrays photoelectrode with enhanced photoelectrocatalytic performance under visible-light irradiation*. Physical Chemistry Chemical Physics.16(28) (2014) 14800-7.
54. Brigden K, Stringer R. Ammonia and Urea Production : Incidents of Ammonia Release From The Profertil Urea and Ammonia Facility, Bahia

Blanca, Argentina. UK: Departement of Biological Science University of Exeter; 2000.

55. Wang R, Xie T, Sun Z, Pu T, Li W, Ao J-P. *Graphene quantum dot modified gC 3 N 4 for enhanced photocatalytic oxidation of ammonia performance*. RSC advances.7(81) (2017) 51687-94.
56. Zhang H, Gu Q-Q, Zhou Y-W, Liu S-Q, Liu W-X, Luo L, et al. *Direct Z-scheme photocatalytic removal of ammonia via the narrow band gap MoS2/N-doped graphene hybrid catalyst upon near-infrared irradiation*. Appl Surf Sci.504 (2020) 144065.
57. Yamazoe S, Okumura T, Hitomi Y, Shishido T, Tanaka T. *Mechanism of photo-oxidation of NH3 over TiO2: Fourier transform infrared study of the intermediate species*. J Phys Chem C.111(29) (2007) 11077-85.